Wavefront modulation and controlling for Lamb waves using surface bonded slice lenses

Zhenhua Tian, and Lingyu Yu

Citation: Journal of Applied Physics **122**, 234902 (2017);
View online: https://doi.org/10.1063/1.4999627
View Table of Contents: http://aip.scitation.org/toc/jap/122/23
Published by the American Institute of Physics

Wavefront modulation and controlling for Lamb waves using surface bonded slice lenses

Zhenhua Tian[1,a)] and Lingyu Yu[2]
[1]*Department of Mechanical Engineering and Material Science, Duke University, Durham, North Carolina 27708, USA*
[2]*Department of Mechanical Engineering, University of South Carolina, Columbia, South Carolina 29208, USA*

(Received 9 August 2017; accepted 14 November 2017; published online 15 December 2017)

There is a growing interest in controlling the propagation of Lamb waves to achieve better performance for structural health monitoring and nondestructive evaluation. In this study, we present new methods of controlling Lamb waves using simple slice lenses through wavefront modulation. The lenses are made of metal slices with designed shapes. Once bonded on plates, the lenses modify the effective plate thickness, and therefore change the Lamb wave characteristics such as the wavenumber and phase velocity, providing convenient ways of modulating wavefront and controlling Lamb waves in plates. Numerically and experimentally, we demonstrated that a straight wavefront A_0 mode can be focused on the desired focal point using a plano-concave aspherical lens. We also demonstrated that the A_0 mode can be steered with different frequency components steered to different directions using a simple prism made of metal slices. The work shows that such simple slice lenses provide easy ways for controlling Lamb waves, and have a great potential for Lamb wave based applications. *Published by AIP Publishing*. https://doi.org/10.1063/1.4999627

I. INTRODUCTION

Lamb waves are elastic waves propagating in plate-like structures guided between two parallel free surfaces.[1] Compared to traditional bulk waves, Lamb waves have the advantage of a long propagation distance with low energy loss.[1] With this merit, Lamb waves have been extensively studied for applications including structural health monitoring (SHM),[2,3] nondestructive evaluation (NDE),[1,4] micro-electro-mechanical systems,[5,6] and acoustofluidics.[7–13] To achieve better performance in these applications, there is a growing interest in controlling the propagation of Lamb waves such as focusing and guiding.

Studies on engineered materials have shown progress in controlling the propagation of flexural waves[14–17] and Lamb waves[18–28] in plates using phononic crystals, metamaterials, and other structures. Wave focusing, guiding, negative refraction, and other capabilities have been achieved. Wu *et al*. demonstrated focusing of A_0 mode Lamb waves in a gradient-index phononic crystal plate.[18] Reboud *et al*. developed phononic crystals, patterned on a disposable chip, to guide Lamb waves for complex fluidic manipulation.[9] Estrada *et al*. proposed phononic plates with inclusions in performed holes, and found that the inclusions had strong effects on the intrinsic modes, leading to mode mixing and band folding.[28] Pierre *et al*. presented negative refraction of A_0 mode Lamb waves through two-dimensional phononic crystals.[20] Jin *et al*. proposed gradient-index phononic plates for simultaneous control of both A_0 and S_0 modes in a broadband frequency region.[25] Besides phononic crystals, metamaterials have shown great capabilities of controlling wave propagation. Chen *et al*. achieved extremely broadband control of flexural waves using an adaptive metamaterial with hybrid shunting circuits.[14] Later, Chen *et al*. developed adaptive gradient-index metamaterials with shunting circuits for enhanced flexural wave sensing.[16] Yan *et al*. proposed surface bonded elastic metamaterials made of planar arrays of lead discs with varying thickness to focus A_0 mode Lamb waves.[19] Zhu *et al*. achieved negative refraction of S_0 mode Lamb waves using single-phase metamaterials with a chiral microstructure.[21] Later, Zhu *et al*. numerically demonstrated subwavelength imaging using an elastic hyperlens made of the single-phase hyperbolic metamaterial.[29] Reviewing these studies, it is realized that most of the work involves a complex material design that requires developing complex periodical phononic crystals or sub-wavelength resonant metamaterials.

Recently, a simple manner of creating engineered lenses by locally reducing the plate thickness has been proposed by Climente *et al*. for controlling flexural waves.[30,31] The method is based on the thickness-dependent property of the flexural wave dispersion relation, and the created gradient-index lenses have shown broadband efficiency and omnidirectional properties. Thickness change has also been applied to achieve negative refraction and focusing of Lamb waves.[32,33] In an aluminum plate with a step change in thickness, Bramhavar *et al*. achieved negative refraction and focusing of high frequency Lamb waves, through the mode conversion from a forward S_2 mode to a backward S_{2b} mode at the step.[32] Later, Philippe *et al*. presented a simple lens made by a thickness trough in an aluminum plate, which can focus the high frequency S_2 mode through the mode conversion between a forward S_2 mode and a backward S_{2b} mode at both edges of the trough.[33] These two studies are

a)Electronic mail: zhenhua.tian@duke.edu

based on the mode conversion between forward waves (with parallel phase and group velocities) and backward waves (with anti-parallel phase and group velocities) at the thickness change. More recently, based on the mode conversion from the S_{2b} mode to S_0 and S_1 modes, Veres *et al.* achieved broad-angle negative reflection and focusing of Lamb waves at a plate edge.[34] Later, Gérardin *et al.* demonstrated that the focusing distance could be changed by tuning the excitation frequency.[35] However, these mode conversion based approaches may have limitation in focusing the A_0 mode, since the A_0 mode does not support backward waves,[36,37] and the conversion from the S_{2b} mode to the A_0 mode is very weak.[35]

In this paper, we present new designs of simple slice lenses to control Lamb waves by modulating the wavefronts. The lenses are slices with designed shapes made of the same material as the host plate, and can be easily added to the host plate using a layer of adhesive (such as hot glue). Such a bonded lens can be easily removed or changed to another one (by melting the hot glue) without distinct damage to the host plate. The bonded lenses slightly increase the effective plate thickness, thus change the wave characteristics such as the wavenumber and phase velocity. Hence, it becomes possible to modulate the wavefronts of Lamb waves transmitting through the lenses and control the propagation of Lamb waves by judiciously designing the shapes of lenses. Through simulations and experiments, we demonstrate that a surface bonded plano-concave aspherical lens can focus a straight wavefront A_0 mode on the focal point of the lens, and a Lamb wave prism can steer the propagation direction of an A_0 mode with different frequency components steered to different directions. We believe such simple, easy to fabricate, and potentially interchangeable lenses with designer shapes provide new ways for controlling Lamb waves, and may be useful for Lamb wave based SHM and NDE applications.

II. DISPERSION PRINCIPLE OF LAMB WAVES

Lamb waves are multi-modal and dispersive. Their dispersion curves can be derived from the Rayleigh-Lamb equations[1]

$$\frac{\tan(qh/2)}{\tan(ph/2)} = -\frac{4k^2qp}{(k^2-q^2)^2} \text{ for symmetric modes,} \quad (1)$$

$$\frac{\tan(qh/2)}{\tan(ph/2)} = -\frac{(k^2-q^2)^2}{4k^2qp} \text{ for anti-symmetric modes,} \quad (2)$$

where

$$p^2 = \frac{\omega^2}{c_L^2} - k^2, \quad q^2 = \frac{\omega^2}{c_S^2} - k^2,$$
$$c_L = \sqrt{\frac{2\mu(1-\nu)}{\rho(1-2\nu)}} \quad \text{and} \quad c_S = \sqrt{\frac{\mu}{\rho}}.$$

k and ω are the wavenumber and circular frequency; c_L and c_S are the velocities of longitudinal and transverse waves; h is the plate thickness; and ρ, μ, and ν are the density, shear modulus, and Poisson's ratio, respectively. By solving the Rayleigh-Lamb equations, the dispersion relation between the frequency $f = \omega/2\pi$ and wavenumber k can be found. The Rayleigh-Lamb equations show that the frequency-wavenumber dispersion relation not only depends on the material properties (ρ, μ, and ν) but also the plate thickness (h).

Figure 1(a) plots the frequency-wavenumber dispersion curves of the fundamental A_0 and S_0 modes in the low frequency range 0–600 kHz for 1 and 2 mm thick aluminum plates. It is seen that the wavenumber difference between S_0 modes in 1 and 2 mm thick plates is nearly negligible, whereas the difference between A_0 modes in 1 and 2 mm thick plates is significant, indicating that different modes may have different sensitivities to the plate thickness. Figure 1(b) shows how the wavenumber varies with respect to the plate thickness (from 1 to 3 mm) at 100 and 300 kHz. We can see that the wavenumbers of S_0 modes remain nearly constant with respect to thickness change at both frequencies. In contrast, the wavenumbers of A_0 modes gradually decrease with the increase of thickness at both frequencies. It further manifests that different Lamb modes may have different sensitivities to the plate thickness and the wavenumber of the A_0 mode will change if the plate thickness is changed. Such a dependence on thickness gives the physical foundation for modulating A_0 Lamb waves through thickness variation. The simple idea is, by adding a slice with a certain thickness made of the same materials as the host plate, the effective plate thickness is changed in the region with the added slice, and the wavenumber of the propagating A_0 mode is therefore changed. The waves can be further

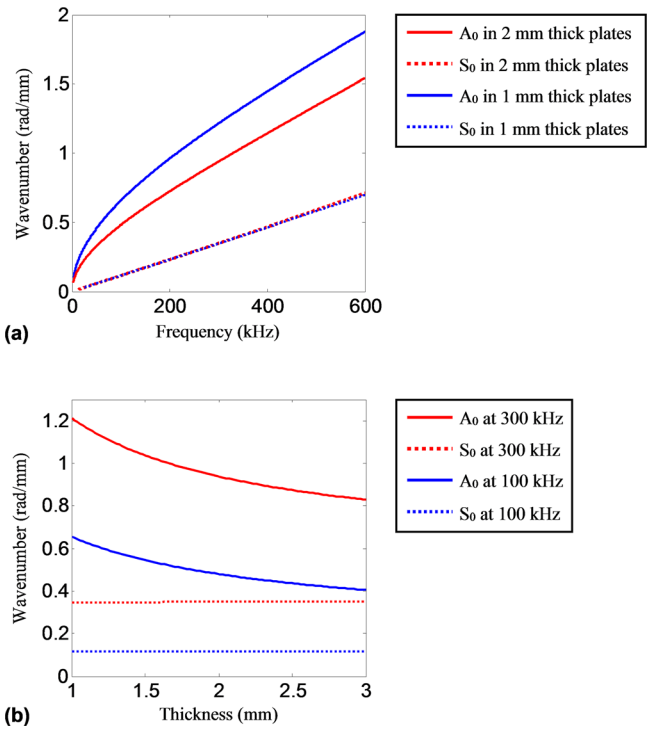

FIG. 1. Wavenumber curves of Lamb waves in aluminum plates. (a) Frequency-wavenumber dispersion curves for A_0 and S_0 modes in 1 and 2 mm thick aluminum plates. (b) Wavenumbers with respect to the plate thickness at 100 and 300 kHz excitation frequencies.

modified based on the shape of the added slice with a constant thickness. Such a simple way of modulating Lamb waves will open a new opportunity to control the propagation of Lamb waves, as well as subsequent SHM and NDE applications.

In practice, the slices can be easily added on the plate using a thin layer of adhesive glues or alike. Note that if the adhesive layer is too thick, the thickness of the adhesive layer should be considered, because it may cause additional wavenumber change as well as induce wave attenuation due to the damping effect.[38] The attenuation is usually very low at low frequencies, while it can be significant at high frequencies.[38] Hence, in our study we make sure that the adhesive layer is thin and focus on the low frequency range (50–200 kHz), such that the wavenumber is nearly not influenced by the adhesive layer and the attenuation effect is relatively low.

III. WAVE FOCUSING BY A PLANO-CONCAVE ASPHERICAL LENS

Focusing Lamb waves into a narrow beam is very useful for Lamb wave based applications such as SHM and NDE.[39,40] The focused waves with higher energy within a narrower beam would offer a better spatial sensing resolution and a higher signal-to-noise ratio for improved damage inspection. In this subsection, a plano-concave aspherical lens is designed for focusing Lamb waves in such a way. Finite element simulations and laser vibrometry experiments are performed, and both results show that a straight wavefront A_0 mode can be focused at the desired location through a plano-concave aspherical lens.

A. Lens design

In optics, the plano-convex and plano-concave aspherical lenses can focus and expand light beams through refraction, respectively. Inspired by the design of optical plano-concave aspherical lens, an elastic plano-concave aspherical lens has been designed to focus Lamb waves in a substrate plate, through wavefront modulation. As shown in Fig. 2, the lens is a slice with a plano-edge B_1B_4 and a concave-edge B_2B_3 made of the same material as the substrate plate. Assuming the plano-concave aspherical lens with thickness h_L is ideally added onto (neglecting the bonding layer) the substrate plate with thickness h_P, the effective plate thickness where the lens is added increases to $h_{PL} = h_P + h_L$. The wavenumbers of Lamb waves in the plate with and without the lens hence become different, denoted as k_{PL} and k_P, respectively.

Assume that the incident Lamb waves propagate in the $+x$ direction in the plate with straight wavefronts parallel to the plano-edge B_1B_4, as illustrated in Fig. 2 and consider only the waves entering the lens from the plano-edge B_1B_4 and exiting from the concave-edge B_2B_3. In order to focus the incident waves on the focal point (F) of the lens, the shape of the lens should be designed such that waves coming from different locations in the wavefront (e.g., C_1 and C_2 given in Fig. 2) would arrive at the focal point at the same time. That is to say, the propagation time along the different paths ($C_1D_1E_1F$ and $C_2D_2E_2F$ in Fig. 2) from the wavefront to the focal point should be the same, as

$$\frac{C_1D_1 + E_1F}{c_P} + \frac{D_1E_1}{c_{PL}} = \frac{C_2D_2 + E_2F}{c_P} + \frac{D_2E_2}{c_{PL}}, \tag{3}$$

where c_{PL} and c_P are the phase velocities in the plate with and without the lens, respectively. Substituting $c_{PL} = \omega/k_{PL}$ and $c_P = \omega/k_P$ into Eq. (3) with k_{PL} and k_P being the wavenumbers in the plate with and without the lens, we can derive

$$k_P E_1F + k_{PL} D_1E_1 = k_P E_2F + k_{PL} D_2E_2. \tag{4}$$

Equation (4) is a generic formula of the relation between wavenumbers and geometry parameters. Using this equation, the plano-concave aspherical lens can be designed to focus incoming planar Lamb waves at its focal point. For this lens, the amplitude of focused waves can be influenced by the shape and size of the lens. In future, analytical studies will be performed to derive an analytical estimation of the focused waves.

B. Finite element simulation

To demonstrate wave focusing using a plano-concave aspherical lens, a finite element simulation has been performed in ANSYS Multiphysics 11.0. The substrate is an aluminum plate with a thickness of 1 mm. As shown in Fig. 3(a), a strip actuator made of Lead Zirconate Titanate (PZT) with the dimensions of 60 mm × 5 mm × 0.3 mm is set at the center of the substrate to generate the A_0 mode with the straight wavefront at 200 kHz, propagating in both $+x$ and $-x$ directions. A plano-concave aspherical lens made of a 1 mm thick aluminum slice is added onto the substrate for

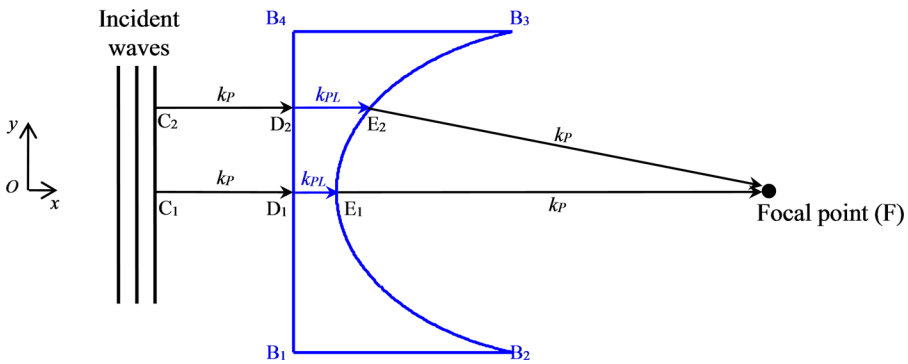

FIG. 2. The principle of focusing Lamb waves using a plano-concave aspherical lens. C_1 and C_2 are two locations on the incident wavefront. The waves from the two locations enter the lens at D_1 and D_2, and then exit the lens at E_1 and E_2, respectively, eventually arriving at the lens' focal point F at the same time.

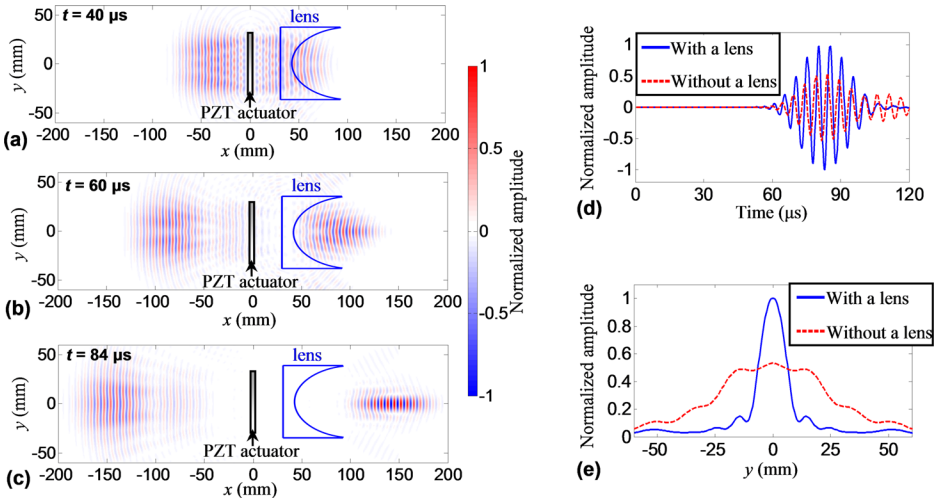

FIG. 3. Focusing the A_0 mode at 200 kHz using a plano-concave aspherical lens. (a), (b), and (c) are the wavefields of out-of-plane displacements at 40, 60, and 84 μs. (d) Comparison between waveforms received at the focal point (at $x = 140$ mm, $y = 0$) with the lens and a reference point (at $x = -140$ mm, $y = 0$) without the lens. (e) Comparison between the wave amplitudes along the lines $x = 140$ mm (with the lens) and $x = -140$ mm (without the lens).

focusing the A_0 mode. The location and dimensions of the plano-concave aspherical lens [illustrated in Fig. 3(a)] satisfy the principle given in Eq. (4) such that the A_0 mode can be focused at the focal point (140, 0) mm.

In the finite element model, the substrate plate and the lens are constructed using three-dimensional (3D) structural elements (with eight nodes in each element and three degrees of freedom at each node). The material properties are given as Young's modulus 71 GPa, Poisson's ratio 0.33, and density 2700 kg/m^3. The 3D coupled field elements (with eight nodes in each element and six degrees of freedom at each node) are selected to build the piezoelectric actuator. The material properties of the piezoelectric actuator can be found in Ref. 41. After the simulation, the wavefields of out-of-plane displacements are acquired for analysis.

Figures 3(a)–3(c) are the simulation results of Lamb wave wavefields at 40, 60, and 84 μs, respectively. Straight wavefront A_0 waves are generated by the strip PZT and propagate outward in both $-x$ and $+x$ directions, as seen in Fig. 3(a). The waves in the $-x$ direction retain straight wavefronts, as propagating further from the actuator. In contrast, waves in the $+x$ direction propagate through the plano-concave aspherical lens, and their wavefronts are gradually modulated and turning focused as they exit the lens [Fig. 3(b)]. At 84 μs, as shown in Fig. 3(c), the waves arrive at the lens focal point (140, 0) mm and are highly focused with the highest amplitude right at the focal point. Figure 3(d) compares the waveforms acquired at the focal point (140, 0) mm using the lens and at a reference point (–140, 0) mm without using the lens. The comparison shows that wave amplitude is increased about two times by the lens. For Lamb waves generated by a rectangular-shaped transducer without using the focusing lens, the generated waves are slightly focused due to the geometric effect of the transducer. This is one reason that the amplitude of waves focused by the lens is only twice that of the amplitude of waves without using the lens. The comparison of amplitudes along the y direction given in Fig. 3(e) shows that waves are more focused in space by using the lens. Besides, the comparisons given above, the wavefield change can also be obtained for further comparison using a wavefield subtraction method,[34] which will be investigated in future.

C. Laser vibrometry experiment

A proof-of-concept laboratory experiment has been performed using a 2024-T3 aluminum plate with dimensions of 305 mm × 305 mm × 1 mm, in order to demonstrate wave focusing by a plano-concave aspherical lens. Figure 4(a) shows a schematic of the experimental setup. A strip PZT actuator (60 mm × 5 mm × 0.3 mm, by Steiner & Martins, Inc.) is bonded on the plate to generate straight wavefront Lamb waves. The center of the PZT is set as the coordinate origin. The PZT excitation is a signal containing 10-count tone bursts at 200 kHz, which are generated by a function generator (model: Agilent 33522B) and then amplified to 30 V by a power amplifier (model: Krohn-Hite 1506). According to the Lamb wave tuning effect,[3] at the excitation frequency of 200 kHz, a strong A_0 mode can be generated by the PZT with a very weak S_0 mode that can be neglected. A plano-concave aspherical lens made of a 1 mm thick aluminum slice [top left, Fig. 4(a)] is bonded on the plate using a thin layer of hot glue. The lens' shape is designed based on Eq. (4) such that the A_0 mode can be focused at the focal point (130, 0) mm. The bonded lens can be easily removed or changed to another one without causing any structural damage by melting the hot glue.

A scanning laser Doppler vibrometer (model: Polytec PSV-400-M2) is used to acquire velocity wavefields of Lamb waves in the scanning area.[42,43] Based on the Doppler Effect,[42,43] the laser vibrometer measures the particle velocity in the direction of the laser beam. In the test, the laser beam is set normal to the plate for measuring the out-of-plane velocity. Using this setup, the A_0 mode can be acquired, since the A_0 mode's out-of-plane motion dominates.[42,43] Through point-by-point scanning at multiple scan points on a predefined scan grid with a spatial interval of 0.5 mm, the laser vibrometer acquires full time-space wavefields of the A_0 mode for wave visualization and further analysis.

Figures 4(b)–4(d) show the wavefields measured by the laser vibrometer at 40, 60, and 80 μs, respectively. These wavefields show that as A_0 waves propagate along the plate, they are gradually focused by the plano-concave aspherical lens. Figure 4(e) plots the distribution of cumulative wave energy,[44] which confirms that the wave energy is focused to a narrow beam with the highest amplitude at the focal point

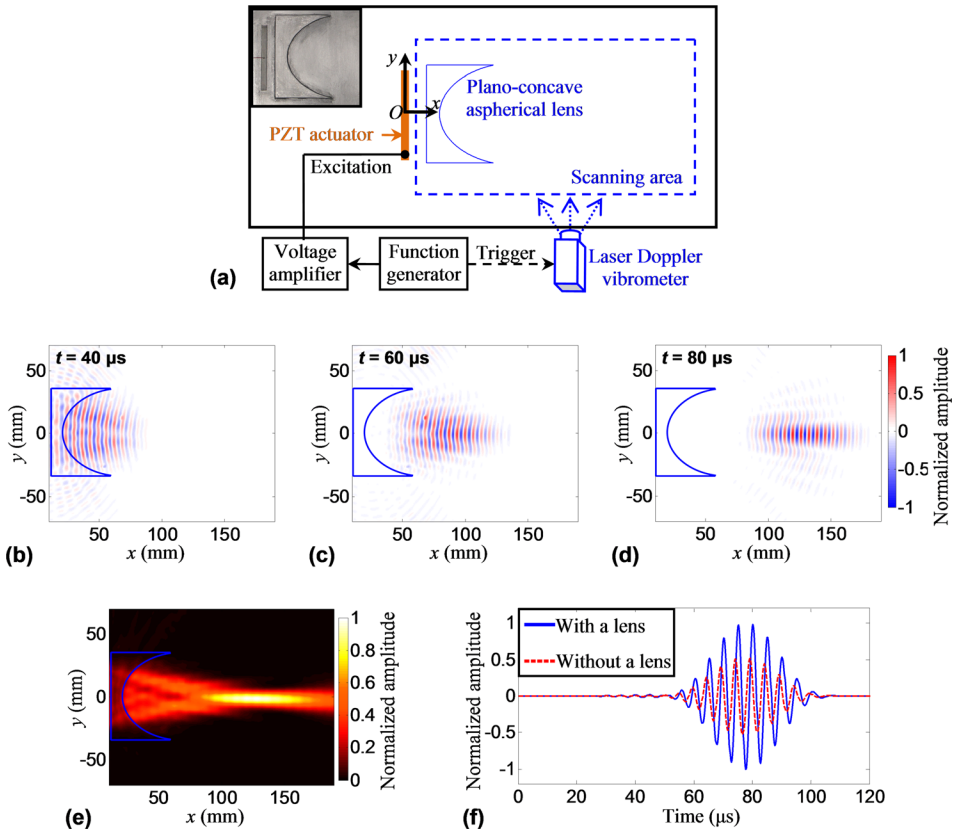

FIG. 4. Focusing the A_0 mode at 200 kHz using a plano-concave aspherical lens. (a) A schematic of the experimental setup and a photo of the lens (top left). (b)–(d) are acquired wavefields (out-of-plane velocities) by the laser vibrometer at 40, 60, and 80 μs. (e) Distribution of the cumulative wave energy. (f) Comparison between waveforms received at the focal point (located at $x = 130$ mm, $y = 0$ mm) with and without the plano-concave aspherical lens.

(130, 0) mm. Figure 4(f) compares the waveforms acquired at the focal point (130, 0) mm with and without using the plano-concave aspherical lens. The comparison shows that the wave amplitude after focusing is nearly twice that of the original amplitude, and proves the focusing capability of the plano-concave aspherical lens. The observations in the experimental results are consistent with those in the simulation results.

IV. WAVE STEERING BY A LAMB WAVE PRISM

Steering the Lamb wave direction toward the suspected area for damage inspection is another interesting area for Lamb wave based SHM and NDE.[39,40] For example, in a complex structure with certain structural discontinuities, the ability of steering waves to bypass those discontinuities is highly desired, so that most of the wave energy can be delivered to the area of interest for damage inspection without being scattered by structural discontinuities. Moreover, Lamb waves are usually selected at certain frequencies in SHM/NDE applications. The frequency-dependent wave steering, therefore, has attracted many researchers' attention, allowing for versatile steering for waves of different frequencies.[45–47] In this subsection, a Lamb wave prism made of a metal slice is designed for steering the Lamb waves. Finite element simulations and laser vibrometry experiments are performed, and both results show the frequency-dependent wave steering of an A_0 mode using a Lamb wave prism.

A. Lens design

The optical dispersive prism can change the propagating direction of light and separate light of different frequencies, due to the frequency dependent refractive index. Inspired by this capability of the optical prism, a Lamb wave prism has been designed to steer the propagation direction of Lamb waves in a substrate plate, as illustrated in Fig. 5. Compared to the design of the focusing lens, the prism design is based on the Snell's law.[1] At the exit of the prism, due to the thickness change, the waves will be refracted. Based on the Snell's law, we can find the relationship between the prism angle α and steering direction θ

$$k_{PL}\cos\alpha = k_P\cos(\alpha+\theta). \tag{5}$$

Equation (5) is a generic formula of the relation between the prism angle α and steering direction θ. Since wavenumbers k_P and k_{PL} depend on the frequency, using Eq. (5), we can further derive the relation between the theoretical steering direction θ and frequency. Figure 6(b) plots the direction θ

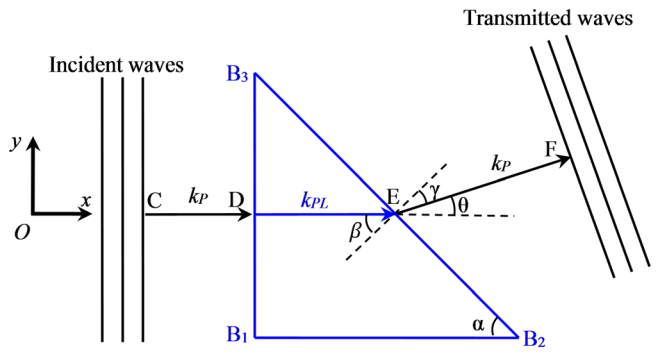

FIG. 5. The principle of steering Lamb waves using a Lamb wave prism. Waves from point C enter the prism at D and then exit the prism at E.

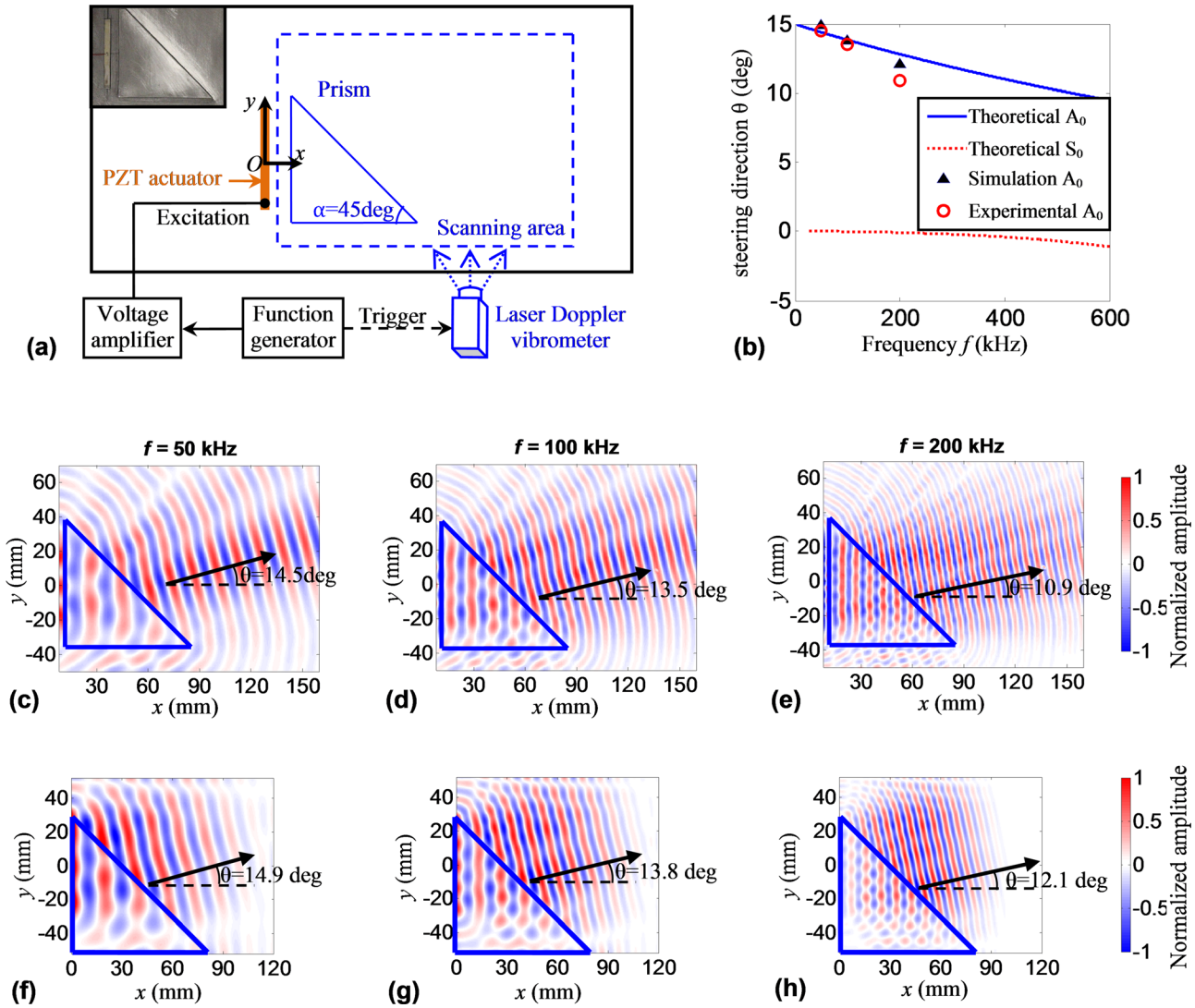

FIG. 6. Steering the A_0 mode using a Lamb wave prism. (a) A schematic of the experimental setup and a photo of the prism (top left). (b) Steering direction θ with respect to the wave frequency when the prism angle $\alpha = 45°$. (c)–(e) are the wavefields (out-of-plane velocities) experimentally acquired by the laser vibrometer at 50, 100, and 200 kHz. In the experimental results, the incident A_0 waves at 50, 100, and 200 kHz are steered to 14.5°, 13.5°, and 10.9°, respectively. (f)–(h) are the wavefields (out-of-plane displacements) obtained through finite element simulations at 50, 100, and 200 kHz. In the simulation results, the incident A_0 waves at 50, 100, and 200 kHz are steered to 14.9°, 13.8°, and 12.1°, respectively.

with respect to the frequency for the case in which a prism with $\alpha = 45°$ made of 1 mm thick aluminum is bonded on a 1 mm thick aluminum substrate plate. It shows that the steering direction θ for the A_0 mode gradually decreases from 15° to 10° as the frequency increases from 0 to 600 kHz, while the θ for the S_0 mode remains nearly zero up to 300 kHz and then shows negligible increase (about 1°) up to 600 kHz, for the reason that the wavenumbers of S_0 modes with and without the prism are almost the same in the low frequency range [Fig. 1(a)].

B. Finite element simulation

To demonstrate the wave steering capability of a Lamb wave prism, a finite element simulation has been performed in ANSYS Multiphysics 11.0. The simulation setup is similar to the setup in Sec. III, except that a prism with an angle $\alpha = 45°$ is used. The location and size of the prism are indicated in Fig. 6(f). The simulation results of wave propagation through the prism at 50, 100, and 200 kHz are shown in Figs. 6(f)–6(h), respectively. As shown in the simulation results, after A_0 waves transmit through the prism, the wavefront becomes skewed and the wave propagation direction is steered. Moreover, the simulation results also reveal that A_0 waves with different frequencies (50, 100, and 200 kHz) are steered to different directions (14.9°, 13.8°, and 12.1°) agreeing well with the theoretical prediction in Fig. 6(b), manifesting that the waves with different frequencies can be directed to different directions.

C. Laser vibrometry experiment

A proof-of-concept laboratory experiment has also been performed. Figure 6(a) plots the overall experimental setup that is nearly the same as the setup given in Fig. 4(a), except that the plano-concave aspherical lens is replaced with a prism. Figure 6(a) (top left) shows a photo of the prism with an angle $\alpha = 45°$, which is made of a 1 mm thick aluminum

slice. A_0 waves at three frequencies 50, 100, and 200 kHz are generated. The out-of-plane velocity wavefields are acquired by the laser vibrometer, shown in Figs. 6(c)–6(e). The wavefields at all frequencies show that the wavefronts become skewed after transmitting through the prism and the wave propagation direction is successfully steered. The side lobes in Figs. 6(c)–6(e) might be induced by the imperfect bonding of the lens. From the experimental results, it can be found that waves at different frequencies (50, 100, and 200 kHz) are steered to different directions (14.5°, 13.5°, and 10.9°). The experimental results agree well with the theoretical prediction in Fig. 6(b), manifesting that the waves with different frequencies can be directed to different directions. The observations in the experimental results are consistent with those in the simulation results.

V. TRANSMISSION, REFLECTION, AND MODE CONVERSION ANALYSIS

In the numerical and experimental studies above, only the transmission A_0 mode is considered. Actually, wave reflection and mode conversion can appear when the incident A_0 mode meets structural discontinuities (such as the boundaries of a lens). To investigate the transmission, reflection, and mode conversion induced by a surface bonded lens, finite element simulations are performed. Figure 7(a) plots the simulation setup. A representative 2D case (cross-section model) is chosen for the simulation. This 2D model considers the main sources of reflection and mode conversion (i.e., ends of the lens). As shown in the simulation setup in Fig. 7(a), a lens (30 mm × 1 mm aluminum) is bonded at the center of a plate substrate (160 mm × 1 mm aluminum). A pure incident A_0 mode is excited at $x = -65$ mm by using antisymmetric out-of-plane point forces on the top and bottom surfaces of the plate. Perfect matching layers (PMLs) are added to the left and right ends of the plate substrate for absorbing Lamb waves, such that no reflections from the ends of plate will present and affect the simulation result. Note that the simulations in this section are performed in COMSOL Multiphysics, since the PML can easily be implemented.

When an incident A_0 mode arrives at the edge of the lens, mode conversion occurs due to the step-like geometric discontinuity created by the sudden thickness change at the bonded lens. Since the boundary conditions at the geometric discontinuity cannot be satisfied by any finite number of Lamb wave modes, all the possible Lamb modes at the excitation frequency will appear.[48] Hence, for our case, the reflection and transmission S_0 waves caused by mode conversion appear at the interface, in addition to the transmission and reflection A_0 waves. The simulation is performed at multiple frequencies from 50 to 350 kHz with a step of 5 kHz. The simulation results (in-plane and out-of-plane displacements) in sensing regions 1 and 2 [shown in Fig. 7(a)] are extracted. To obtain individual wave components for further analysis, Lamb wave decomposition is then applied to the simulation results of sensing regions 1 and 2. Figure 7(b) shows a flow chart of the wave decomposition process. The details of the decomposition method can be found in Ref. 49. Through wave decomposition, the individual components of incident A_0, reflection A_0, and refection S_0 modes can be extracted from the sensing region 1. The individual components of transmission A_0 and S_0 modes can be obtained from the sensing region 2. Among all the individual components, the reflection and transmission S_0 waves are generated from the mode conversion at the ends of the lens. The amplitudes of transmission A_0 and S_0, reflection A_0 and S_0, and incident A_0 modes are denoted as A_{TA}, A_{TS}, A_{RA}, A_{RS}, and A_{IA}, respectively. Note that the wave amplitude A considers both the in-plane A_{IP} and out-of-plane A_{OOP} components, and is defined as $A = \sqrt{A_{IP}^2 + A_{OOP}^2}$. Using the individual wave components, the coefficients of transmission A_0 ($T_A = A_{TA}/A_{IA}$), transmission S_0 ($T_S = A_{TS}/A_{IA}$), reflection A_0

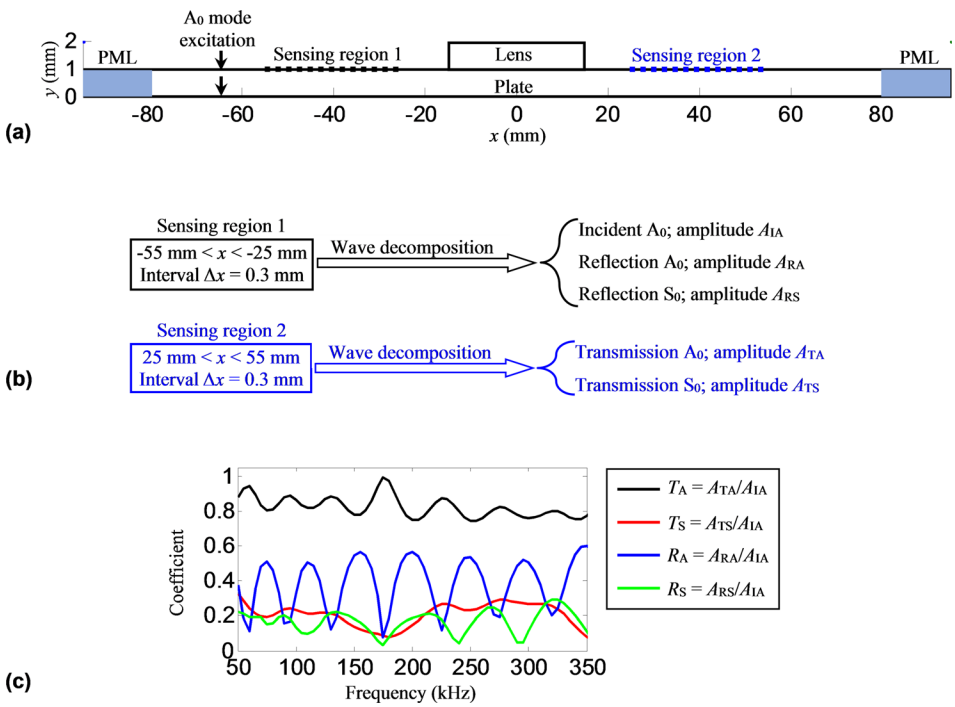

FIG. 7. Transmission, reflection, and mode conversion coefficients obtained through finite element simulation and wave decomposition. (a) A schematic of the simulation setup. (b) Steps for deriving individual wave components through Lamb wave decomposition. (c) Coefficients of transmission A_0 (T_A), transmission S_0 (T_S), reflection A_0 (R_A), and reflection S_0 (R_S) modes.

($R_A = A_{RA}/A_{IA}$), and reflection S_0 ($R_S = A_{RS}/A_{IA}$) can be derived. From the plot of coefficients in Fig. 7(c), it can be seen that although reflection A_0, reflection S_0, and transmission S_0 are present, the transmission A_0 remains at a relatively higher level with a transmission coefficient T_A around 0.8 in the frequency range of 50–350 kHz. This transmission coefficient T_A is used to indicate the amplitude ratio between the transmission and incident A_0 waves for the simplified 2D cross-sectional model. The shape (such as the plano-concave aspherical shape in Sec. III) of the actual lens has not been considered in the 2D model. The transmission coefficient of 0.8 roughly estimates waves that can transmit through the lens to perform further wave manipulation. Given the transmission is 0.8, the plano-concave aspherical lens proposed in Sec. III can still achieve good focusing performance, since waves spread in a large area are concentrated in a small region due to the focusing effect of the lens. As observed in the numerical and experimental results in Sec. III, the amplitude of the focused waves is twice that of the amplitude of waves without focusing.

For lenses proposed in Secs. III and IV, both normal and oblique incident waves could be present. In this section, the numerical study only focuses on the normal incident waves for the first analysis, in order to roughly estimate the transmission, reflection, and mode conversion coefficients related to the surface bonded lens. In future, experiments and 3D simulations with the exact lens geometry will be performed for more precise characterizations.

VI. CONCLUSIONS

Simple slice lenses have been designed for controlling Lamb waves by modulating the wavefront through thickness modification, and the controlling is demonstrated through simulations and experiments. The lenses are designed using slices with optimized designer shapes made of the same material as the substrate. Once the lenses are bonded on the substrate plate, the effective plate thickness is slightly increased and thus wave characteristics such as phase velocity and wavenumber are changed, offering innovative ways of Lamb wave focusing and steering. In addition, a bonded lens can be easily removed or changed to another one without causing structural damage to the substrate. In this paper, a plano-concave aspherical lens is shown to focus the straight wavefront A_0 mode on the focal point of the lens. A Lamb wave prism is shown to steer the propagation direction of the A_0 mode and various directions can be achieved by selecting the excitation frequencies. Our lenses provide easy ways with simple design methodologies for controlling Lamb waves. In addition, the lenses are easy to fabricate and are potentially interchangeable. We believe such designer lenses open new paradigms for controlling Lamb waves and will generate novel applications in SHM and NDE.

The performance of our lens is frequency dependent, due to the dispersion of Lamb waves. Hence, our design requires narrow band excitations, such as 10-cycle tone bursts, to achieve the optimal performance. When a wide bandwidth excitation, such as a 1-cycle tone burst, is adopted, different frequency components can experience different phase modulations in the lens, thus influencing the performance of the lens. Accordingly, the resolution and accuracy for damage detection might be influenced, if the wideband excitation is used. In addition, for experiments in the current study, the slice lenses are bonded on the plates with adhesive layers. Coupling the lenses on the plates using liquid type ultrasonic couplants without bonding them together would be beneficial for practical applications. In future, we will investigate the use of the liquid coupling layer without bonding the lenses on the plates.

Although only the controlling of the A_0 mode is demonstrated in this study, the methodology could be applied to other Lamb modes, whose wavenumber depends on the plate thickness. Further studies on applying the designing methodology for controlling other wave modes will be reported shortly. Second, when the wave frequency goes very high, Lamb waves gradually approximate Rayleigh waves and become insensitive to the thickness change, which potentially causes a frequency limitation to the current design. To overcome this limitation, lenses made of different materials (other than the substrate) could be possibly used to control waves that are not sensitive to thickness change (such as high frequency Lamb waves, Rayleigh waves, and low frequency S_0 mode), since the characteristics of these waves are very sensitive to the material properties. Surface bonded lenses made of different materials for controlling thickness insensitive waves will be investigated as well in the future. Lastly, besides focusing and steering Lamb waves demonstrated in this study, we are currently working on multifunctional and more sophisticated wave controlling through lens combination and wavefront modulation, and the related results will be presented in our future studies.

ACKNOWLEDGMENTS

The authors would like to acknowledge and thank the Department of Energy Grant No. DE-NE 0008400.

[1]J. L. Rose, *Ultrasonic Waves in Solid Media* (Cambridge University Press, Cambridge, 1999).
[2]W. J. Staszewski, C. Boller, and G. R. Tomlinson, *Health Monitoring of Aerospace Structures* (John Wiley & Sons, Chichester, 2004).
[3]V. Giurgiutiu, *Structural Health Monitoring with Piezoelectric Wafer Active Sensors* (Academic Press, Boston, MA, 2008).
[4]J. L. Rose, Proc. SPIE **7983**, 798302 (2011).
[5]M. Kadota, T. Ogami, K. Yamamoto, H. Tochishita, and Y. Negoro, IEEE Trans. Ultrason. Ferroelectr. Freq. Control **57**, 2564 (2010).
[6]H. Jin, J. Zhou, X. L. He, W. B. Wang, H. W. Guo, S. R. Dong, D. M. Wang, Y. Xu, J. F. Geng, J. K. Luo, and W. I. Milne, Sci. Rep. **3**, 2140 (2013).
[7]A. R. Rezk, J. R. Friend, and L. Y. Yeo, Lab Chip **14**, 1802 (2014).
[8]Y. Bourquin, R. Wilson, Y. Zhang, J. Reboud, and J. M. Cooper, Adv. Mater. **23**, 1458 (2011).
[9]J. Reboud, Y. Bourquin, R. Wilson, G. S. Pall, M. Jiwaji, A. R. Pitt, A. Graham, A. P. Waters, and J. M. Cooper, Proc. Natl. Acad. Sci. U. S. A. **109**, 15162 (2012).
[10]A. Haake and J. Dual, Ultrasonics **42**, 75 (2004).
[11]G. Destgeer, B. Ha, J. Park, and H. J. Sung, Anal. Chem. **88**, 3976 (2016).
[12]J. Friend and L. Y. Yeo, Rev. Mod. Phys. **83**, 647 (2011).
[13]X. Y. Ding, P. Li, S. C. S. Lin, Z. S. Stratton, N. Nama, F. Guo, D. Slotcavage, X. L. Mao, J. J. Shi, F. Costanzo, and T. J. Huang, Lab Chip **13**, 3626 (2013).
[14]Y. Y. Chen, G. K. Hu, and G. L. Huang, Smart Mater. Struct. **25**, 105036 (2016).

[15]Y. Y. Chen, J. Hu, and G. L. Huang, J. Intell. Mater. Syst. Struct. **27**, 1337 (2016).
[16]Y. Y. Chen, R. Zhu, M. V. Barnhart, and G. L. Huang, Sci. Rep. **6**, 35048 (2016).
[17]D. Torrent, D. Mayou, and J. Sanchez-Dehesa, Phys. Rev. B **87**, 115143 (2013).
[18]T. T. Wu, Y. T. Chen, J. H. Sun, S. C. S. Lin, and T. J. Huang, Appl. Phys. Lett. **98**, 171911 (2011).
[19]X. Yan, R. Zhu, G. L. Huang, and F. G. Yuan, Appl. Phys. Lett. **103**, 121901 (2013).
[20]J. Pierre, O. Boyko, L. Belliard, J. O. Vasseur, and B. Bonello, Appl. Phys. Lett. **97**, 121919 (2010).
[21]R. Zhu, X. N. Liu, G. K. Hu, C. T. Sun, and G. L. Huang, Nat. Commun. **5**, 5510 (2014).
[22]J. F. Zhao, R. Marchal, B. Bonello, and O. Boyko, Appl. Phys. Lett. **101**, 261905 (2012).
[23]J. C. Hsu, T. T. Wu, and H. S. Hsu, J. Appl. Phys. **113**, 083511 (2013).
[24]M. Carrara, M. R. Cacan, J. Toussaint, M. J. Leamy, M. Ruzzene, and A. Erturk, Smart Mater. Struct. **22**, 065004 (2013).
[25]Y. B. Jin, D. Torrent, Y. Pennec, Y. D. Pan, and B. Djafari-Rouhani, J. Appl. Phys. **117**, 244904 (2015).
[26]R. Zhu, X. N. Liu, G. L. Huang, H. H. Huang, and C. T. Sun, Phys. Rev. B **86**, 144307 (2012).
[27]A. Colombi, P. Roux, and M. Rupin, J. Acoust. Soc. Am. **136**, El192 (2014).
[28]H. Estrada, P. Candelas, F. Belmar, A. Uris, F. J. G. de Abajo, and F. Meseguer, Phys. Rev. B **85**, 174301 (2012).
[29]R. Zhu, Y. Y. Chen, Y. S. Wang, G. K. Hu, and G. L. Huang, J. Acoust. Soc. Am. **139**, 3303 (2016).
[30]A. Climente, D. Torrent, and J. Sanchez-Dehesa, J. Appl. Phys. **114**, 214903 (2013).
[31]A. Climente, D. Torrent, and J. Sanchez-Dehesa, Appl. Phys. Lett. **105**, 064101 (2014).
[32]S. Bramhavar, C. Prada, A. A. Maznev, A. G. Every, T. B. Norris, and T. W. Murray, Phys. Rev. B **83**, 014106 (2011).
[33]F. D. Philippe, T. W. Murray, and C. Prada, Sci. Rep. **5**, 11112 (2015).
[34]I. A. Veres, C. Grünsteidl, D. M. Stobbe, and T. W. Murray, Phys. Rev. B **93**, 174304 (2016).
[35]B. Gérardin, J. Laurent, C. Prada, and A. Aubry, J. Acoust. Soc. Am. **140**, 591 (2016).
[36]C. Prada, D. Clorennec, and D. Royer, J. Acoust. Soc. Am. **124**, 203 (2008).
[37]A. L. Shuvalov and O. Poncelet, Int. J. Solids Struct. **45**, 3430 (2008).
[38]P. T. Birgani, K. N. Tahan, S. Sodagar, and M. Shishesaz, Proc. Inst. Mech. Eng., Part C **229**, 1939 (2015).
[39]V. Giurgiutiu and J. Bao, Struct. Health Monit.—Int. J. **3**, 121 (2004).
[40]L. Y. Yu and Z. H. Tian, Ultrasonics **68**, 43 (2016).
[41]F. Song, G. L. Huang, and K. Hudson, Smart Mater. Struct. **18**, 125007 (2009).
[42]L. Yu and Z. Tian, Struct. Health Monit. **12**, 469 (2013).
[43]F. Li, P. Anzel, J. Yang, P. G. Kevrekidis, and C. Daraio, Nat. Commun. **5**, 5311 (2014).
[44]Z. H. Tian, L. Y. Yu, C. Leckey, and J. Seebo, Smart Mater. Struct. **24**, 105019 (2015).
[45]F. Semperlotti and H. Zhu, J. Appl. Phys. **116**, 054906 (2014).
[46]M. Senesi, B. Xu, and M. Ruzzene, Smart Mater. Struct. **19**, 055026 (2010).
[47]E. Baravelli, M. Senesi, M. Ruzzene, L. De Marchi, and N. Speciale, IEEE Trans. Ultrason. Ferroelectr. Freq. Control **58**, 1430 (2011).
[48]B. Poddar and V. Giurgiutiu, Wave Motion **65**, 79 (2016).
[49]Z. Tian and L. Yu, J. Intell. Mater. Syst. Struct. **25**, 1107 (2014).